ChemPubSoc Europe

DOI: 10.1002/chem.201503424

CHEMISTRY
A European Journal
Communication

Magnetic Properties

Large Hexadecametallic {Mn^{III}–Ln^{III}} Wheels: Synthesis, Structural, Magnetic, and Theoretical Characterization

Kuduva R. Vignesh,[a] Stuart K. Langley,[b] Boujemaa Moubaraki,[b] Keith S. Murray,*[b] and Gopalan Rajaraman*[c]

Abstract: The synthesis, gas sorption studies, magnetic properties, and theoretical studies of new molecular wheels of core type {$Mn^{III}_8Ln^{III}_8$} (Ln = Dy, Ho, Er, Y and Yb), using the ligand $mdeaH_2$, in the presence of *ortho*-toluic or benzoic acid are reported. From the seven wheels studied the {Mn_8Dy_8} and {Mn_8Y_8} analogues exhibit SMM behavior as determined from ac susceptibility experiments in a zero static magnetic field. From DFT calculations a $S = 16$ ground state was determined for the {Mn_8Y_8} complex due to weak ferromagnetic Mn^{III}–Mn^{III} interactions. Ab initio CASSCF + RASSI-SO calculations on the {Mn_8Dy_8} wheel estimated the Mn^{III}–Dy^{III} exchange interaction as $-0.1\ cm^{-1}$. This weak exchange along with unfavorable single-ion anisotropy of Dy^{III}/Mn^{III} ions, however, led to the observation of SMM behavior with fast magnetic relaxation. The orientation of the g-anisotropy of the Dy^{III} ions is found to be perpendicular to the plane of the wheel and this suggests the possibility of toroidal magnetic moments in the cluster. The {Mn_8Ln_8} clusters reported here are the largest heterometallic $Mn^{III}Ln^{III}$ wheels and the largest {3d–4f} wheels to exhibit SMM behavior reported to date.

Investigations of molecular transition metal and lanthanide coordination complexes have attracted great attention over the past two decades because of their beautiful molecular architectures and interesting magnetic properties. Current hot topics in molecular magnetism include single-molecule magnets (SMMs),[1] the magnetocaloric effect,[2] and molecular spin structures used in electronic devices (spintronics).[3] Research into wheel/ring-shaped molecular nanomagnetic materials has gained momentum in recent years because of their potential application as functional materials in nanotechnology, with a particular focus on SMMs, models of one-dimensional chains, and in the study of quantum-size effects.[4] Furthermore, pioneering research by Winpenny and co-workers on polynuclear chromium wheels, incorporating a single heterometallic 3d ion aimed towards providing $S = 1/2$ qubits, has opened up the possibility of quantum computation from such molecular systems.[5] To date, few heterometallic Mn–Ln wheels have been documented, with only one structural example, a family of {$Mn^{III}_4Ln^{III}_4$} complexes.[6] Examples of other 3d–4f wheel motifs include {Fe_4Dy_4}, {Fe_4Ln_2}, {Fe_5Yb_3}, {Fe_3Yb_2}, {$Fe_{16}Ln_4$}, and {$Fe_{10}Ln_{10}$} complexes, all reported by Powell and co-workers.[7] It is noted that the common denominator in the synthesis of the above 3d–4f wheel-type structures is in the use of amine polyalcohol ligands such as triethanolamine and *N*-n-butyldiethanolamine. In recent years some of us have researched, extensively, the coordinating ability of various amine-based polyalcohol pro-ligands, successfully isolating many 3d, 3d–4f, and 4f coordination complexes,[8–10] including a fascinating six-membered Dy^{III}-metallo wheel, which displayed a toroidal magnetic moment.[11] We have therefore used the above precedence and the versatile nature of the pro-ligand *N*-methyldiethanolamine ($mdeaH_2$) towards the formation of novel heterometallic 3d-4f ring/wheel-like molecular complexes. We report herein the synthesis, gas sorption studies, magnetic properties, and theoretical studies of a new molecular wheel of core type {$Mn^{III}_8Ln^{III}_8$} (Ln = Dy, Ho, Er, Y and Yb), using the ligand $mdeaH_2$, in the presence of *ortho*-toluic (*o*-tolH) or benzoic acid (benzH). To the best of our knowledge, the compounds represent the largest Mn^{III}–Ln^{III} heterometallic wheels thus far reported.

The reactions of $Mn(NO_3)_2{\cdot}6H_2O$ and $Ln(NO_3)_3{\cdot}6H_2O$ (Ln^{III} = Dy, Ho, Y, and Er) or $YbCl_3{\cdot}6H_2O$, with $mdeaH_2$ and *ortho*-toluic acid (*o*-tol) or benzoic acid (benz) in acetonitrile, at ambient temperature, followed by the removal of the solvent and redissolution in a MeOH/*i*PrOH or a MeOH/EtOH mixture yielded single crystals of a family of heterometallic-ring complexes of general formulae $[Mn^{III}_8Ln^{III}_8(mdea)_{16}(o\text{-}tol)_8(NO_3)_8]$ (Ln = Dy (**1**); Ho (**2**); Y (**3**) and Yb (**4**)) or $[Mn^{III}_8Ln^{III}_8(mdea)_{16}(benz)_8(NO_3)_8]$ (Ln = Ho (**5**); Y (**6**) and Er (**7**)). For full experimental details, see the Supporting Information. It was found that the nature of the crystallized product was sensitive to the reaction conditions and crystallization solvent employed. If the reaction was

[a] *K. R. Vignesh*
IITB-Monash Research Academy, IIT Bombay
Mumbai, 400076 (India)

[b] *Dr. S. K. Langley, Dr. B. Moubaraki, Prof. K. S. Murray*
School of Chemistry, Monash University,
Victoria, 3800 (Australia)
E-mail: keith.murray@monash.edu

[c] *Prof. G. Rajaraman*
Department of Chemistry
Indian Institute of Technology Bombay
Powai, Mumbai, Maharashtra, 400 076 (India)
Fax: (+91) 22-2576-7152
E-mail: rajaraman@chem.iitb.ac.in

Supporting information, including experimental, crystallographic, and computational details (anisotropy, J and D values), SQUID (ac data and other plots) and TGA instrumentation, TGA images, and powder XRD images, for this article is available on the WWW under http://dx.doi.org/10.1002/chem.201503424.

performed in MeOH, crystals of a planar tetranuclear $\{Mn^{III}_2Ln^{III}_2\}$ 'butterfly' complex (Figure S1 in the Supporting Information) were grown from MeCN in good yield. The magnetic properties of other $\{Mn_2Ln_2\}$ butterfly clusters have been studied by other groups.[12] The same tetranuclear motif was also isolated in the solid state when MeCN was used as the reaction solvent and MeOH (instead of MeOH/*i*PrOH or MeOH/EtOH) as the crystallization solvent. Under the above conditions the isolated butterfly complexes are insensitive to the carboxylic acid used. Though it is often difficult to predict/rationalize the structure of the solid-state product from a self-assembly method of synthesis, it is clear that the nature of the solvent(s) influences the outcome of these reactions. Further to this observation, the reaction is sensitive to the lanthanide ion selected. It is only possible, when using *o*-toluic acid as a co-ligand to isolate the wheel motif when using the later Ln^{III} ions (Dy^{III}–Yb^{III}), whereas when using benzoic acid as the co-ligand, Ho^{III} or a higher atomic number is required. For both co-ligands, however, when the Ln^{III} ion has a lower atomic number than Dy^{III} a different polynuclear product is isolated, the structure and properties of which will be reported in due course.

Compound **1** crystallizes in the tetragonal space group *P*4/*n* (see Table S1 in the Supporting Information for crystallographic details of **1**–**7**) such that the asymmetric unit constitutes a quarter of the molecule. Compounds **2**–**4** crystallize in the monoclinic space group *P*2/*n*, with the asymmetric unit consisting of half of the molecule. Compounds **5**–**7** crystallize in the triclinic space group $P\bar{1}$, with the entire structure found in the asymmetric unit. The molecular structure of **1**–**4** and **5**–**7** are essentially identical, the only difference being the replacement of the *ortho*-toluate ligand for benzoate; therefore, only **1** is described in detail, and is representative of all complexes. Compound **1** is a heterometallic hexadecanuclear $\{Mn^{III}_8Dy^{III}_8\}$ wheel/ring structure (Figure 1). The oxidation states of the ions were determined through charge balance and structural considerations and this is also supported by bond-valence sum (BVS)[13] calculations (Table S2 in the Supporting Information).

The metallic core reveals an alternating arrangement of Mn^{III} and Dy^{III} ions around the ring. The ring is not planar with a zig-zag arrangement of two ions up and two ions down (one Dy^{III} and Mn^{III}) alternating around the ring. At any one time four Mn^{III} and four Dy^{III} ions are roughly in the same plane (Figure 1, bottom). All of the metal ions in the complex are chelated by a $[mdea]^{2-}$ ligand through the N atom and the two O atoms. This resulted in sixteen $[mdea]^{2-}$ ligands overall. For all of these, the two deprotonated O atoms form μ_2-bridges to the two adjacent metal ions, resulting in the ring structure in which adjacent metal centres are primarily linked by pairs of μ_2-alkoxo bridges. The Dy^{III} and Mn^{III} ions are then bridged by eight *syn*,*syn*-*ortho*-toluate ligands. These linkages are found between two hetero-ions that are either both "up" or both "down" around the zig-zag arrangement. Additional peripheral coordination to the Dy^{III} ions is provided by eight chelating nitrate ions, each coordinating to a single Dy^{III} ion through two O atoms. The Mn^{III} centres all display Jahn–Teller octahedral distortions, which are axially elongated, with

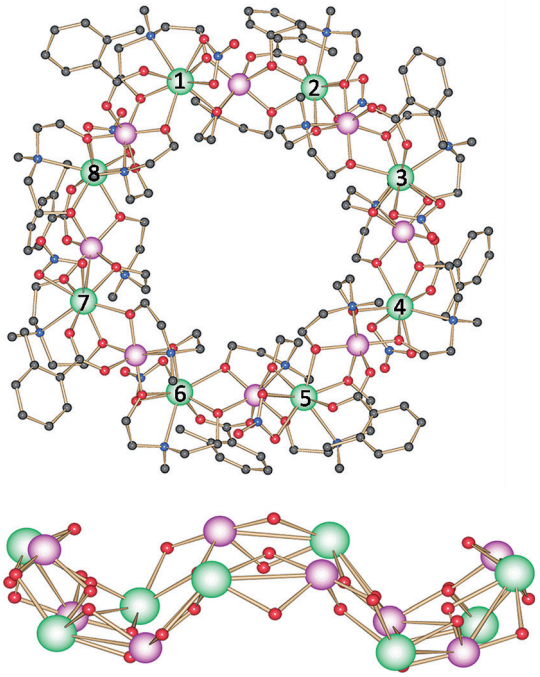

Figure 1. Top: the molecular structure of complex **1**. Bottom: side-view of metal topology found in **1**. The solvent and H atoms are omitted for clarity. Color scheme; Mn^{III}, pink; Dy^{III}, green; O, red; N, blue; C, light grey.

a $\{NO_5\}$ coordination sphere, whereas the $\{NO_7\}$ environments of the Dy^{III} ions reveal distorted triangular dodecahedron geometries. Selected bond lengths and angles for **1** are given in Table S3 in the Supporting Information.

As is to be expected from the high site symmetry of **1**, in the crystal lattice the metallo-rings are aligned with their principal axes co-parallel. The four-fold rotation axes of the molecules are oriented parallel to the crystallographic *c*-axis (Figure S2 in the Supporting Information). As a consequence of the high symmetry it was found that the ring molecules stack on top of each other, forming two types of channel throughout the crystal parallel to the crystallographic *c*-axis (Figure 2). The first channel runs through the centre of the metallo-rings, which are stacked on top of each other. The second lies between four adjacent rings, again running along the *c*-axis. Overall there is a void volume of approximately 43% of the unit cell volume. The packing for **2**–**4** is very similar to compound **1**. However, because of the lower crystallographic symmetry the channel running between adjacent rings is elongated (Figure S3 in the Supporting Information). Upon lowering the crystallographic symmetry for **5**–**7**, the channels found in **1**–**4** are now absent (Figure S4 in the Supporting Information).

The presence of large channels parallel to the tetragonal axis in **1** prompted a study of the thermal behavior and possibility for gas adsorption properties in this compound (see Figure S5 in the Supporting Information for full TGA details). To test for the presence of permanent porosity in the structure, gas adsorption experiments were undertaken using a sample of $\{Mn_8Dy_8\}$ that had been heated under dynamic vacuum at 100 °C overnight. Despite the presence of a plateau in the ther-

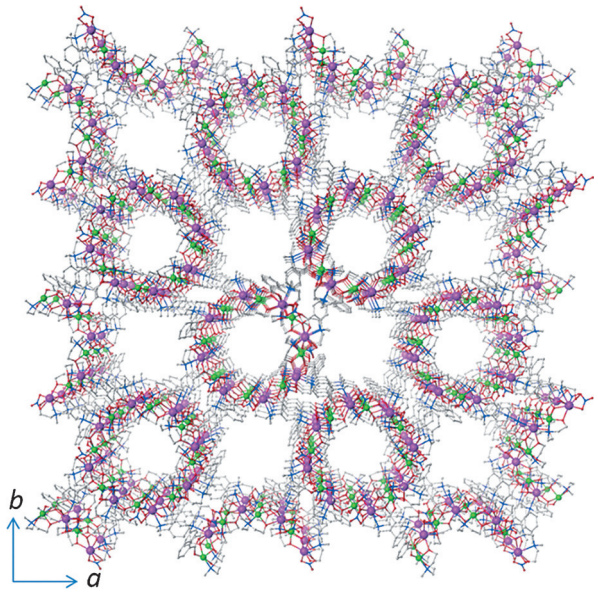

Figure 2. Perspective view of the packing of **1**. It is found that two types of channels are parallel to the crystallographic *c* axis.

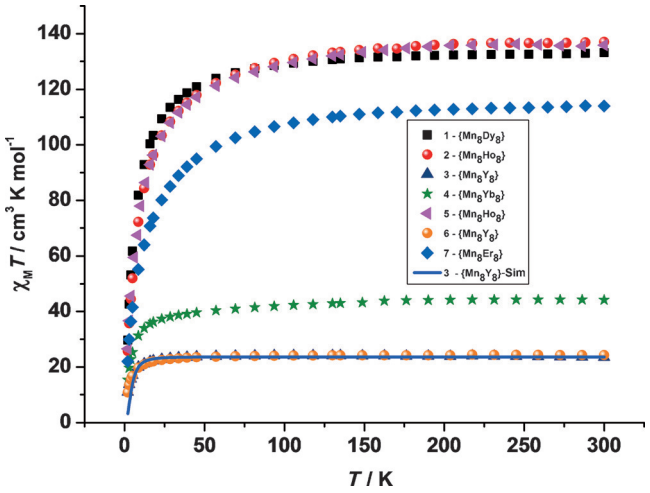

Figure 3. $\chi_M T$ versus T for **1**–**7**, with a dc field of 1 T. The solid blue line is the DFT calculated plot for complex **3**.

mogravimetric analysis plot prior to decomposition, we observed no measurable uptake of N_2 at 77 K in the range 0–0.99 atm after desolvation. Similarly, the uptake of CO_2 at 273 K was considerably lower than would be expected for a permanently microporous molecular material, with a maximum uptake of approximately 8 cc (STP)/g (1.5 wt%) at 1 atm consistent with only particle surface adsorption in an effectively nonporous material (Figure S6 in the Supporting Information). Analysis of the material by X-ray powder diffraction immediately following the gas adsorption experiments suggested that the material had entirely lost crystallinity (Figure S7 in the Supporting Information) during the activation process, presumably leading to pore collapse by slipping of the $\{Mn_8Dy_8\}$ rings.

Magnetic susceptibility measurements on compounds **1**–**7** were carried out in the 300–2 K temperature range in an applied field of 1 T. The variation of the $\chi_M T$ product with temperature revealed similar magnetic susceptibility profiles for all compounds (Figure 3). The magnetic data are summarized in Table S4 in the Supporting Information. The monotonic decrease of $\chi_M T(T)$ of (**1**, **2**, **4**, **5**, and **7**) from room temperature to 1.8 K is indicative of the depopulation of the excited *mJ* Stark levels of the Ln^{III} ions and the likelihood of antiferromagnetic interactions between the Mn^{III} and Ln^{III} ions. For complexes **3** and **6**, containing diamagnetic Y^{III} ions, the $\chi_M T$ product remains constant as the temperature is reduced to $\approx$10 K. This is consistent with negligible spin-orbit effects and the metallic topology in which the paramagnetic Mn^{III} ions are adjacent to the diamagnetic Y^{III} ions around the ring. The magnetic exchange is, therefore, expected to be small due to the large Mn^{III}–Mn^{III} distance (see below). Isothermal *M* versus *H* plots for complexes **1**, **2**, **4** and **7**, shown in Figure S8, reveal gradual increases with increasing *H* at low fields and low temperatures, with *M* then increasing linearly at larger fields, without coming close to a saturation value. This confirms the antiferromagnetic nature of the Mn^{III}–Ln^{III} exchange interactions (see theoretical analysis, see below).

The magnetization dynamics were investigated for each complex by alternating current (ac) susceptibility measurements as a function of both temperature and frequency. A 3.5 Oe oscillating ac field was employed, with a zero static dc field. No SMM behavior was observed above 1.8 K for $\{Mn^{III}_8Ho^{III}_8\}$ (**2**), $\{Mn^{III}_8Yb^{III}_8\}$ (**4**), $\{Mn^{III}_8Ho^{III}_8\}$ (**5**), and $\{Mn^{III}_8Er^{III}_8\}$ (**7**) due to the absence of any frequency and temperature-dependent out-of-phase (χ_M'') signals (Figure S9 in the Supporting Information). A non-zero out-of-phase susceptibility component is observed for $\{Mn^{III}_8Dy^{III}_8\}$ (**1**); however, the peak maxima fall below the operating temperature of the magnetometer (Figure 4), thus indicating SMM behavior but with fast

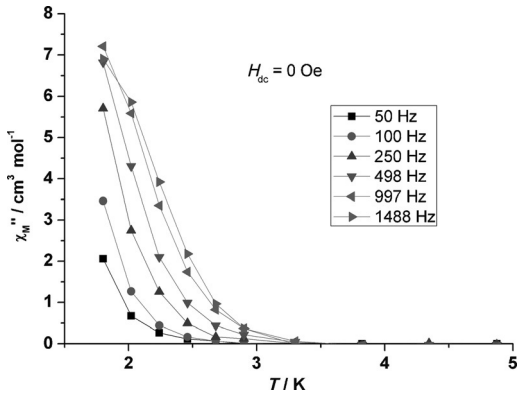

Figure 4. Plot of χ_M'' versus T at the frequencies indicated for **1** with $H_{dc}=0$.

magnetic relaxation times. Interestingly, the same susceptibility profile was observed upon application of a 2000 Oe static dc field (Figure S10 in the Supporting Information). SMM behavior was also observed for the two $\{Mn^{III}_8Y^{III}_8\}$ complexes **3** and **6** (Figure S11 in the Supporting Information), displaying a similar profile, albeit with smaller χ_M'' values compared to **1**.

To fully understand the magnetic properties of **1** and **3**, DFT and ab initio calculations were performed. The magnetic behavior of **1** is determined by the following factors: 1) the single ion anisotropy of the Mn^{III} centres; 2) the single ion anisotropy of the Dy^{III} centres; 3) the Mn^{III}–Dy^{III} nearest-neighbor exchange interactions, and 4) the Mn^{III}–Mn^{III} next-nearest neighbor exchange interaction.[9b] For complex **3**, the prevailing factors are (1) and (4) as the Y^{III} ion is diamagnetic. To estimate the Mn^{III}–Mn^{III} exchange, we have computed the magnetic exchange on the full structure of **3** using the B3LYP/TZV setup (see the Supporting Information for full computational details). The calculation yielded ferromagnetic exchange interactions between the two Mn^{III} centres, with the J value estimated to be $+0.43\ cm^{-1}$. The spin density plot of the HS spin state is shown in Figure 5. It reveals spin polarization along the

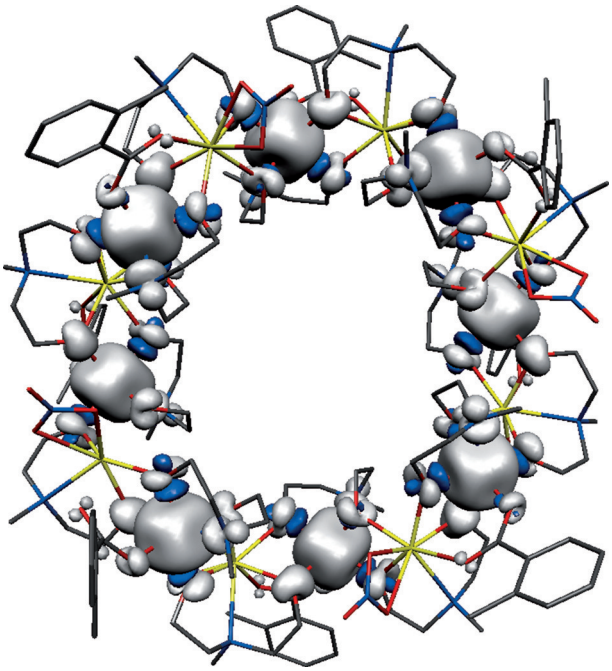

Figure 5. Spin density plot computed for complex **3**. The white and blue colors represent positive and negative spin densities, respectively.

Mn^{III} Jahn–Teller axis and spin delocalization along other axes as previously witnessed for other Mn^{III} ions.[14,15a] A ferromagnetic Mn^{III}–Mn^{III} interaction suggests that complex **3** possesses a $S=16$ ground state, the largest reported for any heterometallic wheel structure; however, larger S values were reported for homoleptic Mn^{III} wheels.[15] The DFT calculated J value with a very small intermolecular interaction, ($zJ=-0.01\ cm^{-1}$) resulted in an excellent fit to the susceptibility data (see Figure S12 in the Supporting Information). Several excited states of lower S values are found to lie only $\approx 2\ cm^{-1}$ higher in energy (see Figure S13 in the Supporting Information). These nested energy levels lead to unsatisfactory fits to the M versus H data. CASSCF calculations using MOLCAS 7.8[16a] reveal that the D values for each Mn^{III} ion lie in the range of -3.4 to $-3.9\ cm^{-1}$,[14a,15a,17] with a small E/D ratio (see the Supporting Information for computational details and Table S5 for the evaluation of the D values using MOLCAS/ORCA suite[18]). These values are in line with that expected for Mn^{III} ions.[14] The Jahn–Teller axes around the wheel are found to be close to perpendicular to each other and this is likely to result in a very small D value for the $S=16$ ground state. This along with the very small exchange parameter J explains the fast magnetic relaxation rate and weak SMM behavior observed for **3**.

As the ac profile for complexes **1** and **3** are different, it rules out the possibility that the SMM behavior in the $\{Mn_8Dy_8\}$ complex **3** originates from the Mn^{III} anisotropy alone. Thus, we have explored the anisotropy of Dy^{III} sites as a second source of magnetic anisotropy. We first examined the structural distortions at individual Dy^{III} sites using SHAPE software.[19] The geometry of each Dy^{III} ion is best described by a triangular dodecahedron. The deviation of 3.2 for Dy1, Dy3, Dy5, and Dy7 and 2.9 for Dy2, Dy4, Dy6, and Dy8 are observed with respect to the ideal triangular dodecahedron. This clearly suggests that there are only two types of non-equivalent Dy^{III} ions (described by odd and even numbers, see Figure 1 for the labeling scheme) in this structure. To fully understand the single-ion relaxation process, we have undertaken CASSCF + RASSI-SO calculations to compute the anisotropy of the Dy^{III} ions using MOLCAS 7.8.[16a] This methodology has been utilized earlier by us to study a number of Dy(III)/Er(III) SMMs.[16b–g] Even though there are only two crystallographic nonequivalent Dy^{III} centers, we performed the calculations on all eight Dy^{III} ions to determine the direction of the local anisotropy axis (see the Supporting Information for computational details). The results of the calculations yield anisotropic g values for Dy1 of $g_x=0.3101$, $g_y=0.8721$, and $g_z=18.5386$, whereas Dy2 yields values of $g_x=0.1414$, $g_y=0.3421$,and $g_z=19.1346$ (Tables S6 and S9 in the Supporting Information). It was then found that the odd-numbered Dy^{III} ions possessed anisotropic values similar to Dy1 and the even-numbered Dy^{III} ions are similar to Dy2 (Table S6 in the Supporting Information), reflecting the structural distortion estimated using SHAPE. For each distinguishable Dy^{III} environment, however, a significant transverse anisotropy is detected, with the transverse component for Dy1 > Dy2. The computed energies of the eight low lying Kramers doublets (KDs) also reflect that there are two types of Dy^{III} ions in the complex (see Tables S7 and S8 in the Supporting Information). The energy gap between the ground and the first excited state KDs are found to be 65.1 and $90.7\ cm^{-1}$ for Dy1 and Dy2, respectively.

A qualitative mechanism for the magnetic relaxation for the Dy1 and Dy2 sites obtained from the ab initio calculations is shown in Figure 6. The KD states are arranged according to the values of the mean absolute value of the matrix elements of the transition magnetic moments between the corresponding states. The calculated barrier to magnetic reorientation suggests a significant quantum tunnelling (QTM) relaxation mechanism between the ground state KDs for Dy1 (and thus all odd-number Dy^{III} ions). For Dy2, on the other hand, the ground-state tunnelling probability is lower, and the relaxation is expected to occur through both ground-state QTM and thermally assisted QTM via the first excited state KDs (also Orbach/

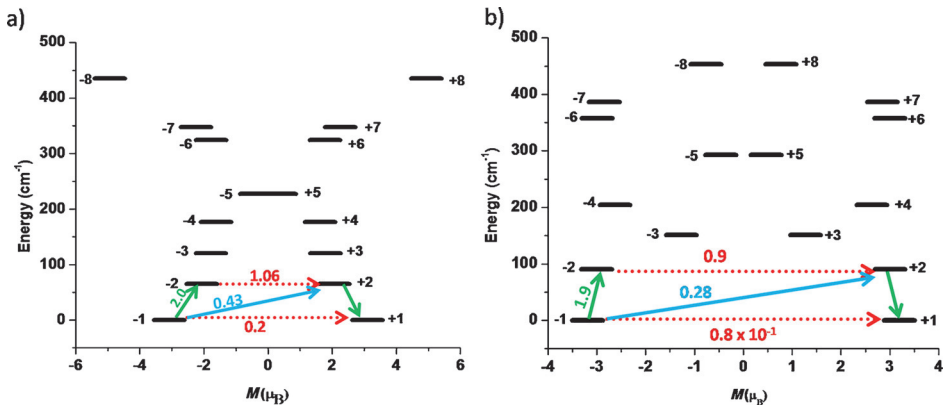

Figure 6. The ab initio computed magnetization blocking barrier for a) the Dy1 site and b) the Dy2 site. The thick black line indicates the Kramers doublets (KDs) as a function of computed magnetic moment. The green/blue arrows show the possible pathway through Orbach/Raman relaxation. The dotted red lines represent the presence of QTM/TA-QTM between the connecting pairs. The numbers provided at each arrow are the mean absolute value for the corresponding matrix element of transition magnetic moment.

Raman process are operational). For this Dy^{III} site, application of a static dc field is expected to quench the QTM between the ground state KD, however the same susceptibility profile was observed upon application of a 2000 Oe dc field suggesting that the observed relaxation is not solely single-ion in origin.

Using the POLY ANISO program[20] the Mn^{III}–Dy^{III} magnetic exchange is estimated to be $-0.1\ cm^{-1}$ (see Figure S14 in the Supporting Information for details). This suggests an alternate spin-up, spin-down for the neighboring ions leading to all the Dy^{III} ions pointing up and Mn^{III} ions pointing down, leading to a spin polarization. The ground-state tunnelling for the exchange coupled state is computed to be small (1.7×10^{-5} in the Supporting Information for details); however, the first excited exchange-coupled state lies just $1.7\ cm^{-1}$ higher in energy, leading to very fast relaxation for the exchange coupled complex. Further to this, the absence of Ising-type Dy^{III} sites (significant g_x and g_y values) with a very weak Mn^{III}–Dy^{III} interaction leading to the Mn^{III} ions acting as independently reorienting magnetic moments at lower temperatures. This acts as a fluctuating magnetic field, which causes the fast reversal of the Dy^{III} magnetization.[21] All of these factors rationalizes the fast relaxation data (QTM relaxation) observed from the ac experiment.

The computed anisotropy direction of the Dy^{III} ions along with the Jahn–Teller axis of the Mn^{III} are shown in Figure 7. The g_{zz} anisotropy at the Dy^{III} sites were found to lie perpendicular to the plane of the wheel and were found to lie along the ~C_4 axis present at the centre of the wheel with some degree of tilt (Figure S15 in the Supporting Information). Due to the asymmetry in the structure (two-up, two-down arrangement), the anisotropy axis of neighboring Dy^{III} ions point towards each other, creating a projected magnetic axis for a pair of Dy^{III} ions, which is expected to lie along the C_4 axis. Although not all the g_{zz} axes create a circular pattern as observed in $\{Dy_3\}$ triangles[22] or the $\{Dy_6\}$ wheel complex,[11b] the projected magnetic moment due to g_{zz} being perpendicular to the plane of the wheel suggests mixed single molecule toroidal (SMT) behavior.[20a,23]

In summary, we report a family of seven Mn^{III}–Ln^{III} wheels that have the largest nuclearity known in the literature. These complexes have been thoroughly characterized by experimental and theoretical studies. The presence of fast magnetic relaxation and weak SMM behavior observed in the $\{Mn_8Dy_8\}$ wheel is attributed to very weak Mn^{III}–Dy^{III} coupling and unfavorable Dy^{III}/Mn^{III} anisotropy. The g_{zz} anisotropy of the Dy^{III} ions in **1** was found to be perpendicular to the plane of the wheel and the computed orientation suggests the possibility of mixed toroidal behavior.

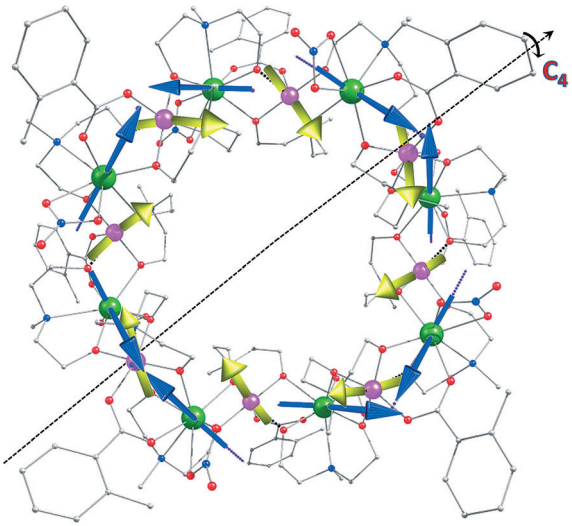

Figure 7. The directions of the local anisotropy axes in the ground Kramers doublet on each Dy site (blue arrows) in **1**. The yellow arrows are JT axes of Mn^{III} ions and the black dotted line is the C_4 axis of **1**.

Acknowledgements

The authors thank Dr. Chris Hawes for gas sorption measurements. G.R. would like to acknowledge the financial support from DST (EMR/2014/000247) India, and IIT Bombay for the high performance computing facility. K.R.V. is thankful to the IITB-Monash Research Academy for a PhD studentship. G.R. and K.S.M. acknowledge the support of an Australia–India Strategic Research Fund (AISRF) grant.

Keywords: ab initio calculations · exchange-coupling · Mn–Ln clusters · single-molecule magnets · wheel-shaped molecule

[1] a) R. Sessoli, D. Gatteschi, A. Caneschi, M. A. Novak, *Nature* **1993**, *365*, 141; b) R. Sessoli, H. L. Tsai, A. R. Schake, S. Wang, J. B. Vincent, K. Folting, D. Gatteschi, G. Christou, D. N. Hendrickson, *J. Am. Chem. Soc.* **1993**, *115*, 1804; c) D. Gatteschi, R. Sessoli, *Angew. Chem. Int. Ed.* **2003**, *42*, 268; *Angew. Chem.* **2003**, *115*, 278.

[2] M. Evangelisti, E. K. Brechin, *Dalton Trans.* **2010**, *39*, 4672.

[3] L. Bogani, W. Wernsdorfer, *Nat. Mater.* **2008**, *7*, 179.

[4] D. Gatteschi, J. Villain, *Molecular Nanomagnets*, Oxford University Press, Oxford, **2006**.

[5] E. J. L. McInnes, S. Piligkos, G. A. Timco, R. E. P. Winpenny, *Coord. Chem. Rev.* **2005**, *249*, 2577.

[6] a) M. Li, Y. Lan, A. M. Ako, W. Wernsdorfer, C. E. Anson, G. Buth, A. K. Powell, Z. Wang, S. Gao, *Inorg. Chem.* **2010**, *49*, 11587; b) M. Li, Y. Lan, A. M. Ako, W. Wernsdorfer, C. E. Anson, G. Buth, A. K. Powell, Z. Wang, S. Gao, *Dalton Trans.* **2010**, *39*, 3375.

[7] a) D. Schray, G. Abbas, Y. Lan, V. Mereacre, A. Sundt, J. Dreiser, O. Waldmann, G. E. Kostakis, C. E. Anson, A. K. Powell, *Angew. Chem. Int. Ed.* **2010**, *49*, 5185; *Angew. Chem.* **2010**, *122*, 5312; b) S. Schmidt, D. Prodius, G. Novitchi, G. E. Kostakis, A. K. Powell, *Chem. Commun.* **2012**, *48*, 9825; c) A. Baniodeh, C. E. Ansona, A. K. Powell, *Chem. Sci.* **2013**, *4*, 4354; d) A. Baniodeh, I. J. Hewitt, V. Mereacre, Y. Lan, G. Novitchi, C. E. Anson, A. K. Powell *Dalton Trans.* **2011**, *40*, 4080; e) A. Baniodeh, Y. Liang, C. E. Anson, N. Magnani, A. K. Powell, A. Unterreiner, S. Seyfferle, M. Slota, M. Dressel, L. Bogani, K. Gob, *Adv. Funct. Mater.* **2014**, *24*, 6280; f) J. R. Machado, A. Baniodeh, A. K. Powell, B. Luy, S. Kramer, G. Guthausen, *ChemPhysChem* **2014**, *15*, 3608.

[8] For example, see: a) S. K. Langley, N. F. Chilton, B. Moubaraki, K. S. Murray, *Dalton Trans.* **2012**, *41*, 9789; b) S. K. Langley, N. F. Chilton, M. Massi, B. Moubaraki, K. J. Berry, K. S. Murray, *Dalton Trans.* **2010**, *39*, 7236.

[9] For example, see: a) S. K. Langley, N. F. Chilton, L. Ungur, B. Moubaraki, L. F. Chibotaru, K. S. Murray, *Inorg. Chem.* **2012**, *51*, 11873; b) S. K. Langley, D. P. Wielechowski, V. Vieru, N. F. Chilton, B. Moubaraki, B. F. Abrahams, L. F. Chibotaru, K. S. Murray, *Angew. Chem. Int. Ed.* **2013**, *52*, 12014; *Angew. Chem.* **2013**, *125*, 12236; c) S. K. Langley, D. P. Wielechowski, V. Vieru, N. F. Chilton, B. Moubaraki, L. F. Chibotaru, K. S. Murray, *Chem. Sci.* **2014**, *5*, 3246; d) N. F. Chilton, S. K. Langley, B. Moubaraki, K. S. Murray, *Chem. Commun.* **2010**, *46*, 7787.

[10] For example, see: a) S. K. Langley, B. Moubaraki, K. S. Murray, *Polyhedron* **2013**, *64*, 255; b) S. K. Langley, B. Moubaraki, K. S. Murray, *Inorg. Chem.* **2012**, *51*, 3947.

[11] a) S. K. Langley, B. Moubaraki, C. M. Forsyth, I. A. Gass, K. S. Murray, *Dalton Trans.* **2010**, *39*, 1705; b) L. Ungur, S. K. Langley, T. N. Hooper, B. Moubaraki, E. K. Brechin, K. S. Murray, L. F. Chibotaru, *J. Am. Chem. Soc.* **2012**, *134*, 18554.

[12] S. Mukherjee, M. R. Daniels, R. Bagai, K. A. Abboud, G. Christou, C. Lampropoulos, *Polyhedron* **2010**, *29*, 54.

[13] a) N. E. Brese, M. O'Keeffe, *Acta Crystallogr. Sect. A* **1991**, *47*, 192; b) W. Liu, H. H. Thorp, *Inorg. Chem.* **1993**, *32*, 4102.

[14] a) G. Rajaraman, M. Murugesu, C. E. Saudo, M. Soler, W. Wernsdorfer, M. Helliwell, C. Muryn, J. Rafterym, S. J. Teat, G. Christou, E. K. Brechin, *J. Am. Chem. Soc.* **2004**, *126*, 15445; b) K. R. Vignesh, S. K. Langley, K. S. Murray, G. Rajaraman, *Chem. Eur. J.* **2015**, *21*, 2881.

[15] a) S. Sanz, J. M. Frost, T. Rajeshkumar, S. J. Dalgarno, G. Rajaraman, W. Wernsdorfer, J. Schnack, P. J. Lusby, E. K. Brechin, *Chem. Eur. J.* **2014**, *20*, 3010; b) R. P. John, K. Lee, M. S. Lah, *Chem. Commun.* **2004**, 2660; c) S. Zartilas, C. Papatriantafyllopoulou, T. C. Stamatatos, V. Nastopoulos, E. Cremades, E. Ruiz, G. Christou, C. Lampropoulos, A. J. Tasiopoulos, *Inorg. Chem.* **2013**, *52*, 12070.

[16] a) F. Aquilante, T. B. Pedersen, V. Veryazov, R. Lindh, *WIREs Comput. Mol. Sci.* **2013**, *3*, 143; b) S. K. Singh, T. Gupta, L. Ungur, G. Rajaraman, *Chem. Eur. J.* **2015**, *21*, 13812; c) C. Das, A. Upadhyay, S. Vaidya, S. K. Singh, G. Rajaraman, M. Shanmugam, *Chem. Commun.* **2015**, *51*, 6137;d) S. K. Singh, T. Gupta, M. Shanmugam, G. Rajaraman, *Chem. Commun.*, **2014**, *50*, 15513 – 15516; e) A. Upadhyay, S. K. Singh, C. Das, R. Mondol, S. K. Langley, K. S. Murray, G. Rajaraman, M. Shanmugam, *Chem. Commun.* **2014**, *50*, 8838 – 8841; f) T. Gupta, G. Rajaraman, *J. Chem. Sci.* **2014**, *126*, 1569 – 1579; g) S. K. Singh, T. Gupta, G. Rajaraman, *Inorg. Chem.* **2014**, *53*, 10835 – 10845.

[17] a) J. Cirera, E. Ruiz, S. Alvarez, F. Neese, J. Kortus, *Chem. Eur. J.* **2009**, *15*, 4078; b) R. Maurice, C. de Graaf, N. Guihery, *J. Chem. Phys.* **2010**, *133*, 084307.

[18] F. Neese, *WIREs Comput. Mol. Sci.* **2012**, *2*, 73.

[19] a) M. Pinsky, D. Avnir, *Inorg. Chem.* **1998**, *37*, 5575; b) J. Cirera, E. Ruiz, S. Alvarez, *Chem. Eur. J.* **2006**, *12*, 3162.

[20] a) L. F. Chibotaru, L. Ungur, A. Soncini, *Angew. Chem. Int. Ed.* **2008**, *47*, 4126; *Angew. Chem.* **2008**, *120*, 4194; b) L. Ungur, W. Van den Heuvel, L. F. Chibotaru, *New J. Chem.* **2009**, *33*, 1224.

[21] A. Bhunia, M. T. Gamer, L. Ungur, L. F. Chibotaru, A. K. Powell, Y. Lan, P. W. Roesky, F. Menges, C. Riehn, G. Niedner-Schatteburg, *Inorg. Chem.* **2012**, *51*, 9589.

[22] J. Tang, I. Hewitt, N. T. Madhu, G. Chastanet, W. Wernsdorfer, C. E. Anson, C. Benelli, R. Sessoli, A. K. Powell, *Angew. Chem. Int. Ed.* **2006**, *45*, 1729; *Angew. Chem.* **2006**, *118*, 1761.

[23] L. Ungur, S.-Y. Lin, J. Tang, L. F. Chibotaru, *Chem. Soc. Rev.* **2014**, *43*, 6894.

Received: August 28, 2015
Published online on September 25, 2015